



**HAL**  
open science

## Dissociative recombination of $\text{CH}_2\text{NH}_2^+$ : a crucial link with interstellar methanimine and Titan ammonia

C. Yuen, Mehdi Ayouz, N. Balucani, C. Ceccarelli, I.F. Schneider, V. Kokoouline

► **To cite this version:**

C. Yuen, Mehdi Ayouz, N. Balucani, C. Ceccarelli, I.F. Schneider, et al.. Dissociative recombination of  $\text{CH}_2\text{NH}_2^+$ : a crucial link with interstellar methanimine and Titan ammonia. *Monthly Notices of the Royal Astronomical Society*, 2019, 484 (1), pp.659-664. 10.1093/mnras/sty3514 . hal-01977242

**HAL Id: hal-01977242**


**<https://hal.science/hal-01977242v1>**

Submitted on 8 Dec 2023

**HAL** is a multi-disciplinary open access archive for the deposit and dissemination of scientific research documents, whether they are published or not. The documents may come from teaching and research institutions in France or abroad, or from public or private research centers.

L'archive ouverte pluridisciplinaire **HAL**, est destinée au dépôt et à la diffusion de documents scientifiques de niveau recherche, publiés ou non, émanant des établissements d'enseignement et de recherche français ou étrangers, des laboratoires publics ou privés.

# Dissociative recombination of $\text{CH}_2\text{NH}_2^+$ : a crucial link with interstellar methanimine and Titan ammonia

C. H. Yuen,<sup>1</sup> M. A. Ayouz,<sup>2</sup> N. Balucani ,<sup>3,4</sup> C. Ceccarelli,<sup>4</sup> I. F. Schneider<sup>5,6</sup> and V. Kokoouline<sup>1</sup>★

<sup>1</sup>Department of Physics, University of Central Florida, Orlando, FL 32816, USA

<sup>2</sup>LGPM, CentraleSupélec, Université Paris-Saclay, 8-10 Rue Joliot Curie, F-91190 Gif-sur-Yvette, France

<sup>3</sup>Dipartimento di Chimica, Biologia e Biotecnologie, Università di Perugia, Via Elce di Sotto 8, I-06123 Perugia, Italy

<sup>4</sup>Institut de Planétologie et d'Astrophysique de Grenoble (IPAG), 120 rue de la Piscine, F-38041 Grenoble, France

<sup>5</sup>LOMC CNRS-UMR6294, Université du Havre, Normandie Université, F-76058 Le Havre, France

<sup>6</sup>Laboratoire Aimé Cotton CNRS-UMR9188, Université Paris-Sud, ENS Cachan, Université Paris-Saclay, F-91405 Orsay, France

Accepted 2018 December 10. Received 2018 December 4; in original form 2018 November 19

## ABSTRACT

Cross-sections for dissociative recombination (DR) and vibrational excitation of the  $\text{CH}_2\text{NH}_2^+$  ion in collisions with electrons are determined theoretically. The corresponding thermally averaged rate coefficients are computed and fitted to analytical formulas. The obtained DR rate coefficient is significantly smaller than the values recently employed in the photochemical models of the upper atmosphere of Titan, which has an important impact on the models that aim to reproduce the Titan ammonia abundance. On the other hand, the present results support the astrophysical models reproducing the abundance of the methanimine ( $\text{CH}_2\text{NH}$ ) detected in massive star formation regions. In these models, the  $\text{CH}_2\text{NH}_2^+$  DR is a major route of formation of this molecule with a high prebiotic potential.

**Key words:** astrochemistry – molecular data – molecular processes – scattering – planets and satellites: atmospheres – ISM: molecules.

## 1 INTRODUCTION

Methanimine,  $\text{CH}_2\text{NH}$ , is an interesting prebiotic molecule which has been detected in several extraterrestrial environments (Woon 2002; Balucani 2012). Its first detection in the interstellar medium dates back to 1973 (Godfrey et al. 1973), while its presence in several high-mass hot cores has been the subject of recent campaigns of detection (Suzuki et al. 2016; Weaver et al. 2017). Until very recently, however, attempts to detect  $\text{CH}_2\text{NH}$  in solar-type star-forming regions failed and only upper limits were given (Suzuki et al. 2016). Only this year Ligterink et al. (2018) have finally detected methanimine towards the solar-type protostar IRAS 16293-2422B, followed by that towards two more young solar-type protostars, IRAS4A and SVS13A (López-Sepulcre et al. submitted), showing that this important small molecule is present in the environments that will eventually form planets, possibly like the Earth.

Methanimine has a very high proton affinity (852.9 kJ mol<sup>-1</sup>, 8.84 eV) and, therefore, its most probable fate is to undergo a proton transfer reaction by interacting with the abundant interstellar ions, namely  $\text{HCO}^+$ ,  $\text{H}_3^+$ , and  $\text{H}_3\text{O}^+$ . In this way, the ion  $\text{CH}_2\text{NH}_2^+$  is

formed. Other  $\text{CH}_2\text{NH}_2^+$  formation routes exist, such as the very fast reaction  $\text{CH}_2^+ + \text{NH}_3 \rightarrow \text{H} + \text{CH}_2\text{NH}_2^+$  (Anicich 1993). Once formed,  $\text{CH}_2\text{NH}_2^+$  can undergo dissociative recombination (DR) and, indeed, this is the only destruction pathway of this ion considered in the two most popular data base of astrochemical networks: KIDA (Wakelam et al. 2012) and UMIST (McElroy et al. 2013).

The recommended rate coefficients and relative product branching ratios are given in Table 1. The overall rate coefficients differ by a factor of two between the KIDA and UMIST data bases. In addition, given the different product branching ratios, according to the UMIST data base, 50 per cent of  $\text{CH}_2\text{NH}_2^+$  is recycled back to neutral methanimine, while in the KIDA data base only 24 per cent of  $\text{CH}_2\text{NH}_2^+$  does so. Therefore, according to the scheme proposed by the UMIST data base, protonation, and DR mildly affect the overall amount of neutral methanimine. According to the KIDA data base, instead, the loss of neutral methanimine is more significant.

Another environment where methanimine and protonated methanimine are important is the upper atmosphere of Titan, the massive moon of Saturn. The Ion and Neutral Mass Spectrometer (INMS) on-board Cassini orbiter provided important insights into the ionosphere of Titan. Among the detected ions, the signal at the charge-to-mass ratio of 30 was attributed to the presence of  $\text{CH}_2\text{NH}_2^+$  (Vuitton, Yelle & Anicich 2006). From the detection of protonated

★ E-mail: viatcheslav.kokoouline@ucf.edu

**Table 1.** Summary of the recommended reaction rate coefficients and branching ratios of the DR of  $\text{CH}_2\text{NH}_2^+$ . The first column reports the reference of the values quoted in the next three columns: the reaction products, and the  $\alpha$  and  $\beta$  values for the reaction rate coefficient as a function of the temperature  $T$ , where the usual formalism,  $k(T) = \alpha \times (T/300)^\beta \exp(-\gamma/T)$ , is used. Note that all the quoted reactions are barrierless, so that  $\gamma$  is equal to zero. The references codes are: Y2010 (Yelle et al. 2010); V2018 (Vuitton et al. 2018); K2009 (Krasnopolsky 2009); D2016 (Dobrijevic et al. 2016). The last line reports the overall value found in this work.

References	Products	$\alpha$	$\beta$
UMIST	$\text{CH}_2\text{NH} + \text{H}$	$1.5 \times 10^{-7}$	-0.5
	$\text{CH}_2 + \text{NH}_2$	$1.5 \times 10^{-7}$	-0.5
	<b>Overall</b>	$3.0 \times 10^{-7}$	-0.5
KIDA	$\text{CH}_2\text{NH} + \text{H}$	$1.5 \times 10^{-7}$	-0.5
	$\text{CH}_2 + \text{NH}_2$	$1.5 \times 10^{-7}$	-0.5
	$\text{HCN} + \text{H} + \text{H}_2$	$3.0 \times 10^{-7}$	-0.5
	$\text{CN} + \text{H}_2 + \text{H}_2$	$3.0 \times 10^{-8}$	-0.5
	<b>Overall</b>	$6.3 \times 10^{-7}$	-0.5
Y2010 and V2018	$\text{CH}_2\text{NH} + \text{H}$	$0.5\text{--}1.4 \times 10^{-6}$	-0.7
	$\text{CH}_2 + \text{NH}_2$	$0.5\text{--}1.4 \times 10^{-7}$	-0.7
	$\text{HCN} + \text{H} + \text{H}_2$	$0.5\text{--}1.4 \times 10^{-7}$	-0.7
	<b>Overall</b>	$1.5\text{--}4.2 \times 10^{-7}$	-0.7
	<b>Preferred</b>	$2.1 \times 10^{-6}$	-0.7
K2009	$\text{CH}_2 + \text{NH}_2$	$3.0 \times 10^{-7}$	-0.5
D2016	$\text{CH}_2\text{NH} + \text{H}$	$9.0 \times 10^{-7}$	-0.7
	$\text{CH}_2 + \text{NH}_2$	$3.0 \times 10^{-7}$	-0.7
	$\text{HCN} + \text{H} + \text{H}_2$	$1.2 \times 10^{-6}$	-0.7
	$\text{HNC} + \text{H} + \text{H}_2$	$3.0 \times 10^{-7}$	-0.7
	$\text{H}_2\text{CN} + \text{H} + \text{H}$	$3.0 \times 10^{-7}$	-0.7
	<b>Overall</b>	$3.0 \times 10^{-6}$	-0.7
This work	<b>Overall, upper limit</b>	$4.65 \times 10^{-7}$	-0.5

methanimine, it has been confirmed that  $\text{CH}_2\text{NH}$  is relatively abundant in the upper atmosphere of Titan, thus substantially confirming the prediction of the photochemical model by Lavvas, Coustenis & Vardavas (2008), even though it overestimated its abundance. Clearly, some destruction pathways were missing in that model and it was speculated that methanimine can polymerize and contribute to the formation of the haze aerosols (Lavvas et al. 2008). This suggestion was later disproved by Skouteris et al. (2015) as dimerization of neutral methanimine was found to be characterized by high-energy barriers. Barrierless processes, instead, are possible for its ionic forms, such as methanimine cation ( $\text{CH}_2\text{NH}^+$ ) or protonated methanimine (Skouteris et al. 2015). The reactions between protonated or ionic methanimine and one neutral methanimine molecule could also account for the formation of polymethylenimine observed in experiments on interstellar or cometary ice analogues (Bernstein et al. 1995; Vinogradoff et al. 2013; Skouteris et al. 2015).

Finally, it has been shown that the DR of  $\text{CH}_2\text{NH}_2^+$  is a pivotal step in the formation of ammonia in the upper atmosphere of Titan around 950–1500 km of altitude (Yelle et al. 2010). According to the proposition by Yelle et al. (2010), indeed, ammonia (which has also been identified via the detection of its protonated form  $\text{NH}_4^+$ ) is formed mainly by the reaction between the  $\text{NH}_2$  and  $\text{H}_2\text{CN}$  radicals. In turn, the main route of  $\text{NH}_2$  formation was suggested to be the DR of  $\text{CH}_2\text{NH}_2^+$ . Since there were no experimental or theoretical data about the DR of  $\text{CH}_2\text{NH}_2^+$ , the rate coefficient of this process was estimated using data on complex hydrocarbon

ions. The adopted value is quite larger than that used in the KIDA and UMIST data bases, being  $2.1 \times 10^{-6} \text{ cm}^3 \text{ s}^{-1}$ , with equal probabilities for the three possible branches  $\text{CH}_2\text{NH} + \text{H}$ ,  $\text{CH}_2 + \text{NH}_2$ , and  $\text{HCN} + \text{H} + \text{H}_2$  (see Table 1). A sensitivity analysis was also performed by using values among  $1.5$  and  $4.2 \times 10^{-7} (T/300)^{-0.7}$ ; the adopted value of  $2.1 \times 10^{-6}$  is the one that better reproduces the  $\text{CH}_2\text{NH}_2^+$  observed densities. Notably, in the model of Krasnopolsky (2009), a lower value for the rate coefficient of the  $\text{CH}_2\text{NH}_2^+$  DR was used and ammonia density could not be reproduced. Also, Dobrijevic et al. (2016) employed a similar value for the overall rate coefficient, but the product branching ratio was quite different, with the dominant channel being the formation of  $\text{HCN} + \text{H} + \text{H}_2$ . In the various models, the trend with the temperature is also different, with the  $\beta$  factor varying between  $-0.7$  and  $-0.5$ .

Clearly, a reliable value for the rate coefficient of the DR of  $\text{CH}_2\text{NH}_2^+$  is important and needed. In this paper, we present a theoretical investigation of this process, which has allowed us to provide an upper limit for the total rate coefficient of the  $\text{CH}_2\text{NH}_2^+$  DR. The implications of the present calculations in the chemistry of extraterrestrial environments will also be addressed.

## 2 THEORETICAL APPROACH

Since  $\text{CH}_2\text{NH}_2^+$  is a closed-shell ion, it requires a highly energetic incoming electron to form a doubly excited resonant dissociative state of the neutral. Consequently, the low-energy electrons are more likely to be captured into vibrationally excited  $\text{CH}_2\text{NH}_2$  Rydberg resonances, which are strongly pre-dissociated. This process is known as the *indirect* DR.

Although there are 12 degrees of freedom for the internal motion, the formalism for indirect DR from Fonseca dos Santos et al. (2014) can be applied in a straightforward manner. Within this approach, the rotational structure and couplings are neglected, the propensity rule for the vibrational electron capture  $\Delta v = +1$  is assumed (Herzberg & Jungen 1972; Jungen & Pratt 2009), as well as the fact that, once the electron is captured by the ion, pre-dissociation is much faster than auto-ionization. These assumptions worked well for most polyatomic ions so far explored (Mikhailov et al. 2006; Jungen & Pratt 2009; Schneider, Pop & Jungen 2012; Douguet et al. 2012b). Consequently, the probability of capturing the incoming electron is equal to the sum of probabilities of vibrational excitation (VE) of all normal modes of the ionic target by one quanta. However, when the collision energy is large enough to vibrationally excite certain normal modes of the ionic target, we assume that the neutral complex will eject an electron and that we are left with a vibrationally excited ion, rather than dissociation products of the neutral.

The computation of the scattering matrix for VE or de-excitation (VDE)  $S_{v_i \leftarrow v_i'}$  relies on the vibrational frame transformation (Chang & Fano 1972)

$$S_{v_i \leftarrow v_i'} = \sum_{l'l'\lambda\lambda'} \langle \chi_{v_i} | S_{ll'\lambda\lambda'}(\vec{Q}) | \chi_{v_i'} \rangle, \quad (1)$$

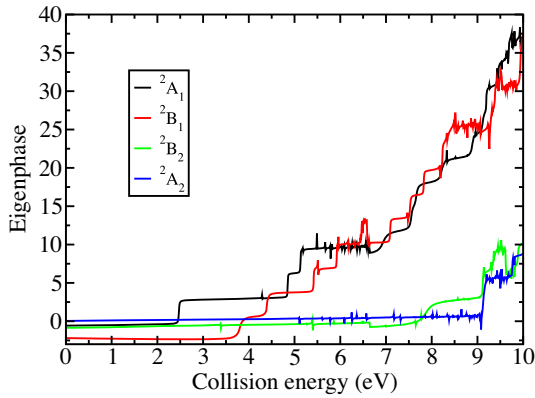
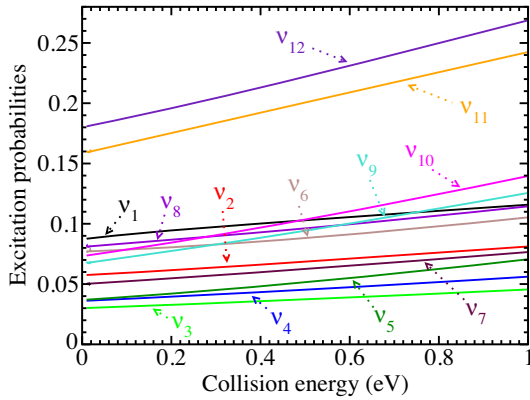
where  $S_{ll'\lambda\lambda'}$  is the fixed-nuclei scattering matrix for initial and final orbital angular momenta  $l, l'$ , and their projections on a body-fixed (molecular symmetry) axis  $\lambda, \lambda'$  at geometry  $\vec{Q}$ .

Based on the propensity rule  $\Delta v = +1$  and on the harmonic approximation, the cross-section for VE of one quanta for the  $i^{\text{th}}$  normal mode writes:

$$\sigma_{v_i+1 \leftarrow v_i'}(\epsilon) = \frac{\pi \hbar^2}{2m_e \epsilon} (v_i' + 1) \theta(\epsilon - \hbar\omega_i) P_i, \quad (2)$$

**Table 2.** Vibrational frequencies of  $\text{CH}_2\text{NH}_2^+$  in  $\text{cm}^{-1}$  ( $10^{-3}$  Hartree). OPB means out-of-plane bending and IPB means in plane bending.

Mode	This study	Thackston & Fortenberry (2018)
$\omega_1$ $\text{NH}_2$ OPB ( $B_1$ )	954.41 (4.343)	950.8
$\omega_2$ $\text{CH}_2$ - $\text{NH}_2$ antisymmetric IPB ( $B_2$ )	977.70 (4.45)	965.9
$\omega_3$ $\text{CH}_2$ - $\text{NH}_2$ twist ( $A_2$ )	1104.23 (5.025)	1086.1
$\omega_4$ $\text{CH}_2$ OPB ( $B_1$ )	1182.22 (5.38)	1165.7
$\omega_5$ $\text{CH}_2$ - $\text{NH}_2$ symmetric IPB ( $B_2$ )	1388.64 (6.319)	1368.0
$\omega_6$ $\text{CH}_2$ scissor ( $A_1$ )	1486.69 (6.765)	1463.1
$\omega_7$ $\text{NH}_2$ scissor ( $A_1$ )	1629.97 (7.417)	1603.3
$\omega_8$ $\text{C}=\text{N}$ stretch ( $A_1$ )	1801.85 (8.2)	1769.3
$\omega_9$ $\text{C}-\text{H}$ symmetric stretch ( $A_1$ )	3212.76 (14.62)	3166.2
$\omega_{10}$ $\text{C}-\text{H}$ antisymmetric stretch ( $B_2$ )	3337.03 (15.19)	3292.5
$\omega_{11}$ $\text{N}-\text{H}$ symmetric stretch ( $A_1$ )	3546.23 (16.14)	3500.6
$\omega_{12}$ $\text{N}-\text{H}$ antisymmetric stretch ( $B_2$ )	3653.78 (16.63)	3606.9

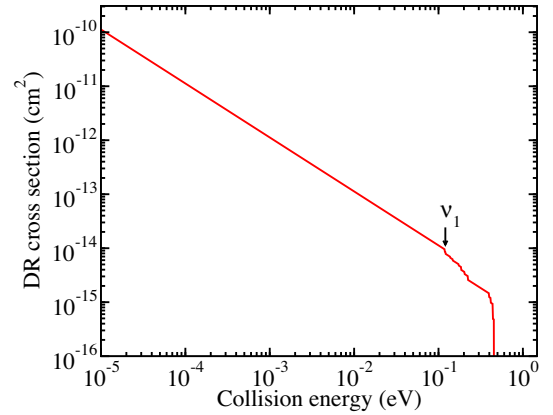

**Figure 1.** Energy dependence of eigenphases of different irreducible representations for the  $\text{CH}_2\text{NH}_2^+ + e^-$  collisions.

**Figure 2.** Excitation probabilities  $P_i$  of equation (3). Each normal mode is indicated by the arrow with the same colour. Due to the smooth energy dependence, excitation probabilities can be fitted with quadratic functions.

$$P_i = \frac{1}{2} \sum_{l'l'\lambda\lambda'} \left| \frac{\partial S_{ll'\lambda\lambda'}}{\partial q_i} \right|_{q_0}^2, \quad (3)$$

where  $v'_i$  is the initial vibrational quantum number,  $m_e$  and  $\epsilon$  are the mass and energy of the incoming electron,  $q_i$  are the dimensionless normal coordinates,  $\omega_i$  are frequencies for different vibrational modes, and  $q_0$  is the equilibrium geometry of the target.  $P_i$  can be

**Table 3.** Coefficients from the curve fitting  $P_i = a_i + b_i E + c_i E^2$  ( $E$  in Hartree).

Mode	$a_i$	$b_i (E_h^{-1})$	$c_i (E_h^{-2})$
$P_1$	$8.798 \times 10^{-2}$	$8.818 \times 10^{-1}$	-3.560
$P_2$	$5.712 \times 10^{-2}$	$5.881 \times 10^{-1}$	1.908
$P_3$	$3.000 \times 10^{-2}$	$3.703 \times 10^{-1}$	1.441
$P_4$	$3.602 \times 10^{-2}$	$4.640 \times 10^{-1}$	2.287
$P_5$	$3.675 \times 10^{-2}$	$6.819 \times 10^{-1}$	6.551
$P_6$	$7.668 \times 10^{-2}$	$4.654 \times 10^{-1}$	8.670
$P_7$	$4.995 \times 10^{-2}$	$6.389 \times 10^{-1}$	2.370
$P_8$	$8.097 \times 10^{-2}$	$7.505 \times 10^{-1}$	4.383
$P_9$	$6.710 \times 10^{-2}$	1.362	6.354
$P_{10}$	$7.298 \times 10^{-2}$	1.499	8.722
$P_{11}$	$1.586 \times 10^{-1}$	2.275	$3.501 \times 10^{-1}$
$P_{12}$	$1.796 \times 10^{-1}$	2.172	7.174


**Figure 3.** The DR cross-section as a function of the collision energy. For energies above 0.1 eV several vibrationally excited channels are open. As a result, the DR cross-section decreases in a stepwise manner.

interpreted as excitation probabilities from the ground vibrational state. The Heaviside step function  $\theta(\epsilon - \hbar\omega_i)$  opens the VE channel when the collision energy is larger than one quanta of the vibrational energy for the  $i^{\text{th}}$  normal mode.

In the case where the ionic target is vibrationally excited, the cross-section for VDE for the  $i^{\text{th}}$  normal mode is

$$\sigma_{v'_i-1 \leftarrow v'_i}(\epsilon) = \frac{\pi \hbar^2}{2m_e \epsilon} v'_i P_i \quad (4)$$

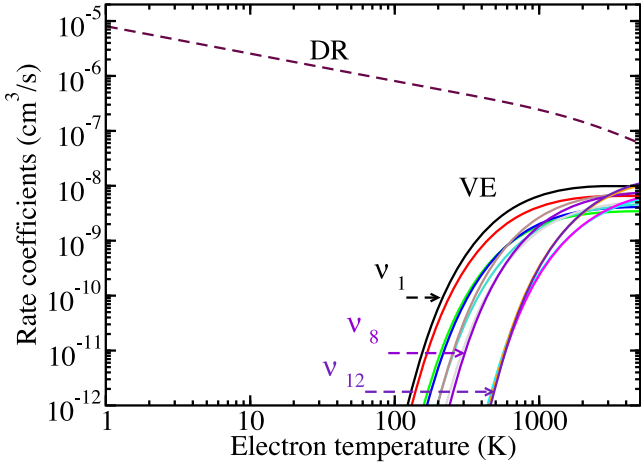


**Figure 4.** The DR (dashed line) and VE (solid lines) rate coefficients for target ion  $\text{CH}_2\text{NH}_2^+$  in the ground vibrational state. To avoid overcrowded labelling in the figure, labels for three VE curves are given only. The lines for all VE rates cross the abscissa in the order of increasing number labelling the modes (and increasing energy) as in Table 2. For  $T < 400$  K, the DR and VE rate coefficients behave as  $T^{-1/2}$  and  $T^{-1/2}\exp(-\hbar\omega_i/k_bT)$ , respectively. At higher temperatures, as VE becomes more probable, the DR rate coefficient decreases faster than  $T^{-1/2}$ .

within the harmonic approximation. There is no Heaviside function in this formula, since VDE is not subject to energy threshold effect.

Finally, the full DR cross-section, resulting from the temporary captures in all the accessible Rydberg states, is given by

$$\langle \sigma_{\{v'\}}^{DR}(\epsilon) \rangle = \frac{\pi \hbar^2}{2m_e \epsilon} \sum_i^{12} (v'_i + 1) \theta(\hbar\omega_i - \epsilon) P_i, \quad (5)$$

where  $\{v'\}$  denotes the collection of initial vibrational quantum numbers of all the normal modes and the Heaviside step function subtracts the contribution from the normal modes which are energetically allowed to excite.

### 3 RESULTS AND DISCUSSION

The electronic structure and vibrational frequencies are calculated using the MOLPRO suite (Werner et al. 2008). The basis set cc-pVQZ is used for all atoms. The electronic energy is obtained using multireference configuration interaction method with Hartree–Fock orbitals. The first two  $a_1$  orbitals are frozen in the calculation, while the complete active space has five  $a_1$ , two  $b_1$ , and three  $b_2$  orbitals.  $\text{CH}_2\text{NH}_2^+$  has 16 electrons, such that it has a closed-shell ground state configuration  $^1A_1$ . Upon optimizing the geometry, we found that it has  $C_{2v}$  symmetry at the equilibrium. C and N atoms are connected to two H atoms forming an angle with  $117^\circ$  and  $121.1^\circ$ , respectively, while C–H and N–H bond length are 1.01 and 1.078 Å. C and N atoms are connected with a double bond with bond length 1.271 Å. We computed the frequencies of the normal modes using the same complete active space. Table 2 displays the frequencies and symmetries of the 12 vibrational modes.

Using the QUANTEMOL-N suite (Tennyson et al. 2007), we obtained the fixed-nuclei energy-dependent reactance matrices for the  $\text{CH}_2\text{NH}_2^+ + e^-$  collisions. The matrices are diagonalized and eigenphases are derived. Fig. 1 shows the eigenphases sum of the  $\text{CH}_2\text{NH}_2^+ + e^-$  system for different irreducible representations at the equilibrium position of the target ion. The eigenphases are smooth below 2.5 eV, where the first electronic resonance appears

for the  $^2A_1$  state. The absence of electronic resonances at low collision energies justifies the indirect DR approach.

The fixed-nuclei reactance matrices are then used to compute scattering matrices  $S$ . In the next step, the derivatives of  $S$ -matrix in equations (3)–(5) with respect to the normal coordinates are computed. The derivatives are obtained using the finite difference method calculated from two values,  $q_i = 0.01$  and  $0.1$ , for the displacements in each mode. The obtained excitation probabilities  $P_i$  of equation (3) are shown in Fig. 2. Since all  $P_i$  curves are smooth with respect to the collision energy, each curve can be fitted with a quadratic function. Table 3 lists the fitted parameters for each normal mode.

With the excitation probabilities, we calculated the DR cross-section according to equation (5). Fig. 3 shows the DR cross-section for target in its vibrationally ground state as a function of collision energy. For energies above 0.1 eV, the cross-section drops in stepwise manner because the scattered electron excites the vibrational level of the ionic target by one quanta and consequently leaves with a smaller kinetic energy.

Due to the simple form of the excitation probabilities and assuming that the collision energy follows Maxwell–Boltzmann distribution, rate coefficients can be computed analytically as

$$\alpha_{v'_i}^{VE}(T) = \sqrt{2\pi} (v'_i + 1) \frac{\hbar^2}{m_e^{3/2}} \left[ (a_i + \hbar\omega_i b_i + (\hbar\omega_i)^2 c_i) / \sqrt{k_b T} + (b_i + 2\hbar\omega_i c_i) \sqrt{k_b T} + 2c_i (k_b T)^{3/2} \right] \exp\left(-\frac{\hbar\omega_i}{k_b T}\right), \quad (6)$$

$$\alpha_{v'_i}^{VDE}(T) = \sqrt{2\pi} v'_i \frac{\hbar^2}{m_e^{3/2}} \left[ \frac{a_i}{\sqrt{k_b T}} + b_i \sqrt{k_b T} + 2c_i (k_b T)^{3/2} \right], \quad (7)$$

and

$$\alpha_{v'_i}^{DR}(T) = \sqrt{2\pi} \frac{\hbar^2}{m_e^{3/2}} \sum_i^{12} (v'_i + 1) \left\{ 2c_i \left[ 1 - \exp\left(-\frac{\hbar\omega_i}{k_b T}\right) \right] (k_b T)^{3/2} + \left[ b_i - (b_i + 2\hbar\omega_i c_i) \exp\left(-\frac{\hbar\omega_i}{k_b T}\right) \right] \sqrt{k_b T} + \left[ a_i - (a_i + \hbar\omega_i b_i + (\hbar\omega_i)^2 c_i) \exp\left(-\frac{\hbar\omega_i}{k_b T}\right) \right] / \sqrt{k_b T} \right\}, \quad (8)$$

where  $a_i$ ,  $b_i$ , and  $c_i$  are the fitted parameters from Table 3. Using the above analytical fits and the parameters of Table 3, the obtained rate coefficients will be expressed in atomic units. Note that the temperature  $k_b T$  will also be in atomic units. To convert the obtained values to the units of  $\text{cm}^3 \text{s}^{-1}$ , the above rate coefficients should be multiplied by a factor of  $6.126159 \times 10^{-9}$ .

Fig. 4 displays the thermally averaged VE and DR rate coefficients as functions of temperature for the initial ground vibrational state,  $v'_i = 0$ . For  $T < 400$  K, the rate coefficients behave as  $1/\sqrt{T}$ . Since the exponent factor  $\exp(-\hbar\omega_i/k_b T)$  is much smaller than 1, the DR rate coefficient can be approximated as  $4.65 \times 10^{-7} (300/T)^{0.5} \text{ cm}^3 \text{ s}^{-1}$ . For  $T > 400$  K, the VE rate coefficients increase rapidly from about  $10^{-10}$  to  $10^{-8} \text{ cm}^3/\text{s}$ , while the DR rate coefficient decrease faster than  $T^{-1/2}$ .

### 4 UNCERTAINTY ESTIMATIONS

There are two main identifiable sources of uncertainty in the DR and VE rate coefficients obtained using the theoretical approach

**Table 4.** Parameters of three different scattering models. Different basis and electronic configurations are used for normal modes with different point group symmetries. The symbols in the parenthesis indicate the number of frozen orbitals and number of active orbitals.

Model	$C_1(\omega_3)$	$C_s(x=0)(\omega_2, \omega_5, \omega_{10}, \omega_{12})$	$C_s(y=0)(\omega_1, \omega_4)$	$C_{2v}(\omega_6, \omega_7, \omega_8, \omega_9, \omega_{11})$
1	cc-pVTZ,(5a 6a)	cc-pVQZ,(2a', 0a'' 8a', 2a'')	cc-pVQZ,(2a', 0a'' 7a', 3a'')	cc-pVQZ,(4a <sub>1</sub> , 0b <sub>1</sub> , 1b <sub>2</sub> , 0a <sub>2</sub>  2a <sub>1</sub> , 2b <sub>1</sub> , 2b <sub>2</sub> , 0a <sub>1</sub> )
2	cc-pVTZ,(5a 6a)	cc-pVTZ,(2a', 0a'' 8a', 2a'')	cc-pVTZ,(2a', 0a'' 7a', 3a'')	cc-pVTZ,(4a <sub>1</sub> , 0b <sub>1</sub> , 1b <sub>2</sub> , 0a <sub>2</sub>  2a <sub>1</sub> , 2b <sub>1</sub> , 2b <sub>2</sub> , 0a <sub>1</sub> )
3	cc-pVTZ,(5a 6a)	cc-pVQZ,(2a', 0a'' 8a', 2a'')	cc-pVQZ,(2a', 0a'' 7a', 3a'')	cc-pVQZ,(2a <sub>1</sub> , 0b <sub>1</sub> , 0b <sub>2</sub> , 0a <sub>2</sub>  5a <sub>1</sub> , 2b <sub>1</sub> , 3b <sub>2</sub> , 0a <sub>1</sub> )

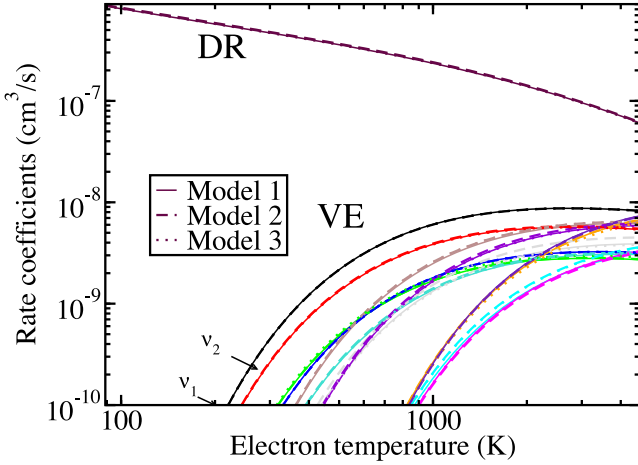


**Figure 5.** The figure shows DR and VE rate coefficients obtained with three different scattering models. Model 1 is the one used in the final calculations discussed above. The differences between results obtained in the three models are very small, about 1–2 per cent, such that the rate coefficients obtained with the three models are almost indistinguishable in the figure.

described above. The most important source is the approximation (the capture model) that once the electron is captured into a vibrational Rydberg resonance associated with a closed vibrationally excited channel, the  $\text{CH}_2\text{NH}_2^+ + e^-$  system will dissociate with 100 per cent probability. In reality, there is a chance that such vibrational Rydberg resonances will autoionize and will not lead to dissociation. It is beyond the scope of this study to make a complete uncertainty assessment of the approximation for the case of  $\text{CH}_2\text{NH}_2^+ + e^-$  collisions, but one can compare with uncertainties evaluated in previous studies of smaller molecular ions, such as  $\text{H}_3^+$ ,  $\text{HCO}^+$ ,  $\text{NH}_4^+$ ,  $\text{H}_3\text{O}^+$ ,  $\text{CH}^+$  (Mikhailov et al. 2006; Douguet et al. 2012b; Douguet, Kokouline & Orel 2012a; Fonseca dos Santos et al. 2014). It was estimated that the probability of autoionization of vibrational Rydberg resonances in these closed-shell ions is of the order of 10–20 per cent compared to the probability of dissociation. For larger ions the probability should be smaller. Therefore, it is reasonable to assume that the corresponding uncertainty in the present DR calculations is below 20 per cent. The relative uncertainty in the VE rate coefficients is about the same as the DR uncertainty.

The second identifiable source of uncertainty is the particular scattering model used in the calculation. To assess the associated uncertainty, we vary several parameters of the models. The three sets of parameters are listed in Table 4. The above results are obtained using the parameters of model 1. The parameters of models 2 and 3 are only slightly different from the parameters of model 1. Calculating the derivatives of the  $S$ -matrix of equation (3), the parameters for  $\omega_3$  mode were unchanged in all three models. The changes in calculations for other modes are indicated in Table 4. Although such variations in the parameters of the model

are rather modest, they give an idea about the sensitivity of the obtained results with respect to the uncertainty in the choice of the parameters.

Complete calculations of DR and VE cross-sections and rate coefficients were performed with these changes. The obtained rate coefficients are shown in Fig. 5. Relative differences between results obtained in the three models are 1–2 per cent. Therefore, the uncertainty associated with the choice of the scattering model is negligible compared to the capture-model approximation. This suggests that the overall uncertainty of the present theoretical rate coefficients is below 20 per cent.

## 5 ASTROPHYSICAL IMPLICATIONS

The value for the DR rate coefficient obtained in this work at  $T < 400$  K is much more in line with the values employed in the UMIST and KIDA data bases rather than with the new estimates by Yelle et al. (2010) and Dobrijevic et al. (2016). In Yelle et al. (2010), the DR rate coefficient has been overestimated by a factor of three. Moreover, the value obtained with our method is well below the lower limit value of  $1.5 \times 10^{-6}$  that still allows the model to predict with a reasonable approximation the detected abundance of  $\text{CH}_2\text{NH}_2^+$ . Therefore, other processes have to be at work in the Titan atmosphere.

This characterization does not permit us to derive the product branching ratio. We note, however, that it is unlikely that all three dissociation channels have the same branching ratio at low collision energy as in Yelle et al. (2010). Another energetically possible dissociation channel, neglected by Yelle et al. (2010) but considered in Dobrijevic et al. (2016), is  $\text{H}_2\text{CN} + \text{H}_2$ . This can also affect the rate coefficient of formation of  $\text{NH}_3$ .

Considering the interstellar  $\text{CH}_2\text{NH}$ , Suzuki et al. (2016) published an extensively modelling of its predicted abundance. They found that methanimine is mainly formed in the gas phase rather than on grain surfaces, and that the  $\text{CH}_2\text{NH}_2^+$  DR is a major formation route, surpassed by the  $\text{NH} + \text{CH}_3$  reaction only. The relative importance of these two reactions depends on the specific model and evolution time-scale, going from unity to a factor ten at most. Our new computations substantially confirm the value used in Suzuki et al. (2016), assuming that the branching ratios used by these authors are correct.

## 6 CONCLUSIONS

To summarize, we reported the first value for the total DR cross-section and thermally averaged rate coefficient of  $\text{CH}_2\text{NH}_2^+$ , which is the largest polyatomic ions considered for DR so far.

The value is in line with the suggestions of the two most popular astrochemical data bases, KIDA, and UMIST, while it is significantly smaller than those recently employed in the photochemical models of the upper atmosphere of Titan (see Table 1). This has an impact on the models that aim to reproduce the Titan ammonia abundance (e.g. Yelle et al. 2010; Vuitton et al. 2018).

On the other hand, models aiming at reproducing the abundance of the methanimine detected in massive star formation regions show that the  $\text{CH}_2\text{NH}_2^+$  DR is a major route of formation of this molecule with a high prebiotic potential (Suzuki et al. 2016). It will then be important to understand whether it has a similar or even larger role in the abundance of methanimine in lower mass, solar-type star-forming regions, where the connection with biotic molecules would be even more important. The recent discoveries of methanimine in such regions warrant a further study, where the branching ratios of the  $\text{CH}_2\text{NH}_2^+$  DR should be elucidated too.

## ACKNOWLEDGEMENTS

This work was supported by the National Science Foundation Grant No. PHY-1806915 and the Chateaubriand Fellowship of the Office for Science and Technology of the Embassy of France in the United States. It has also received funding from the European Research Council (ERC) under the European Union's Horizon 2020 research and innovation program, for the Project 'The Dawn of Organic Chemistry (DOC)', grant agreement No. 741002. IFS acknowledges the French Programme National 'Physique et Chimie du Milieu Interstellaire' (PCMI) of CNRS/INSU with INC/INP, co-funded by CEA and CNES.

## REFERENCES

- Anicich V. G., 1993, *J. Phys. Chem. Ref. Data*, 22, 1469  
 Balucani N., 2012, *Chem. Soc. Rev.*, 41, 5473  
 Bernstein M. P., Sandford S. A., Allamandola L. J., Chang S., Scharberg M. A., 1995, *ApJ*, 454, 327  
 Chang E. S., Fano U., 1972, *Phys. Rev.*, 6, 173  
 Dobrijevic M., Loison J., Hickson K., Gronoff G., 2016, *Icarus*, 268, 313  
 Douguet N., Kokoouline V., Orel A. E., 2012a, *J. Phys. B: At. Mol. Opt. Phys.*, 45, 051001  
 Douguet N., Orel A. E., Greene C. H., Kokoouline V., 2012b, *Phys. Rev. Lett.*, 108, 023202  
 Fonseca dos Santos S., Douguet N., Kokoouline V., Orel A. E., 2014, *J. Chem. Phys.*, 140, 164308  
 Godfrey P., Brown R., Robinson B., Sinclair M., 1973, *Astrophys. Lett.*, 13, 119  
 Herzberg G., Jungen C., 1972, *J. Mol. Spectrosc.*, 41, 425  
 Jungen C., Pratt S. T., 2009, *Phys. Rev. Lett.*, 102, 023201  
 Krasnopolsky V. A., 2009, *Icarus*, 201, 226  
 Lavvas P., Coustenis A., Vardavas I., 2008, *Planet. Space Sci.*, 56, 67  
 Ligterink N. F. W., Terwisscha van Scheltinga J., Taquet V., Jørgensen J. K., Cazaux S., van Dishoeck E. F., Linnartz H., 2018, *MNRAS*, 480, 3628  
 McElroy D., Walsh C., Markwick A., Cordiner M., Smith K., Millar T., 2013, *A&A*, 550, A36  
 Mikhailov I. A., Kokoouline V., Larson A., Tonzani S., Greene C. H., 2006, *Phys. Rev.*, 74, 032707  
 Schneider I., Pop N., Jungen C., 2012, *Phys. Rev.*, 86, 062706  
 Skouteris D., Balucani N., Faginas-Lago N., Falcinelli S., Rosi M., 2015, *A&A*, 584, A76  
 Suzuki T., Ohishi M., Hirota T., Saito M., Majumdar L., Wakelam V., 2016, *ApJ*, 825, 79  
 Tennyson J., Brown D. B., Munro J. J., Rozum I., Varambhia H. N., Vinci N., 2007, *J. Phys.: Conf. Series*, 86, 012001  
 Thackston R., Fortenberry R. C., 2018, *Icarus*, 299, 187  
 Vinogradoff V., Fray N., Duvernay F., Briani G., Danger G., Cottin H., Theulé P., Chiavassa T., 2013, *A&A*, 551, A128  
 Vuitton V., Yelle R. V., Anicich V. G., 2006, *ApJ*, 647, L175  
 Vuitton V., Yelle R., Klippenstein S., Hörst S., Lavvas P., 2018, *Icarus* (In press)  
 Wakelam V., et al., 2012, *ApJS*, 199, 21  
 Weaver S. L. W. et al., 2017, *ApJS*, 232, 3  
 Werner H.-J., Knowles P. J., Lindh R., Manby F. R., Schütz M. et al., 2008, in *MOLPRO*, version 2008.3, a package of ab initio programs  
 Woon D. E., 2002, *ApJ*, 571, L177  
 Yelle R. V., Vuitton V., Lavvas P., Klippenstein S., Smith M., Hörst S., Cui J., 2010, *Faraday Discuss.*, 147, 31

This paper has been typeset from a  $\text{\TeX}/\text{\LaTeX}$  file prepared by the author.